Hindawi
Advances in Civil Engineering
Volume 2019, Article ID 3714381, 15 pages
https://doi.org/10.1155/2019/3714381

Research Article

Surface Subsidence Prediction Method for Coal Mines with Ultrathick and Hard Stratum

Hongkai Han,[1,2] **Jialin Xu**,[1,2] **Xiaozhen Wang**,[1,2,3] **Jianlin Xie**,[2] **and Yantuan Xing**[1,4]

[1]*School of Mines, China University of Mining and Technology, Xuzhou 221116, China*
[2]*State Key Laboratory of Coal Resource and Safe Mining, China University of Mining and Technology, Xuzhou 221116, China*
[3]*State Key Laboratory of Groundwater Protection and Utilization in Coal Mining, China Energy Group, Beijing 100011, China*
[4]*Disaster Prevention Research Institute, Shaanxi Changwu Tingnan Coal Co., Ltd, Xianyang 713602, China*

Correspondence should be addressed to Xiaozhen Wang; 1193401538@qq.com

Received 21 December 2018; Accepted 10 March 2019; Published 7 April 2019

Academic Editor: Giovanni Biondi

Overburden conditions consisting of ultrathick and hard stratum (UTHS) are widespread in China and other countries, but existing surface subsidence prediction methods ignore the strong impact of UTHS on surface subsidence. They are thus not applicable for surface subsidence prediction for coal mining with the presence of UTHS. We conducted actual measurements of surface and UTHS subsidence in the Tingnan Coal Mine. The results showed that under the UTHS mining condition, the required gob dimension is much larger than the empirical value when the surface reaches sufficient mining and that the actual measured maximum value of surface subsidence is much smaller than the empirical value. The UTHS subsidence is approximately equal to the surface subsidence. The movement of UTHS has a strong impact on surface subsidence and has a controlling function for it. It was proposed that surface subsidence could be approximately predicted by calculating the UTHS subsidence. The UTHS movement characteristics were studied using Winkler's theory of beams on an elastic foundation, the subsidence prediction equation of the main sections in the strike and dip directions was obtained under different mining dimensions, and the subsidence prediction equation of any arbitrary cross section parallel to the two main sections was established. Then, the surface subsidence prediction method for coal mining with the presence of UTHS was developed, and the influences of UTHS thickness, strength, and layer position on the surface subsidence were discussed. The Tingnan Coal Mine was taken as an example, and the subsidence curves of the strike and dip main sections were calculated using different mining dimensions. Subsequently, the surface subsidence after the mining of working faces 204, 205, 206, and 207, respectively, was predicted, and the prediction method was verified by comparing the results with the measured surface subsidence results of working faces 204, 205, and 206.

1. Introduction

Coal mining inevitably leads to movement of overburden strata and surface subsidence, and surface subsidence can result in massive lowering of the surface, damage to construction works, geological disasters, and damage to farmland, which have strong impacts on the ecological environment and the normal production of human society [1–6]. Precise prediction of surface subsidence has great significance to land planning in mining areas, mining design of coal resources, safety evaluation of surface facilities in mining areas, prevention of geological disasters, and realization of sustainable development. Numerous methods [6–22] for predicting the subsidence caused by underground coal mining have been developed. The profile function and influence function methods are now widely employed in all methods due to their practicality and ease of use [23]. For conditions in which the topsoil is thick and the overburden strata include no ultrathick and hard stratum (UTHS), the aforementioned methods have relatively high precision for predicting surface subsidence. However, for overburden strata with

UTHS, the prediction results often differ greatly from measured results. For example, when mining under the ultrathick igneous rock of the Haizi Coal Mine, the predicted maximum surface subsidence value obtained using influence function methods was significantly larger than the measured value (1270 mm versus 457 mm, respectively) [24]. This occurs because most of the above prediction methods consider the overburden strata as a homogenous medium [25]. When the composition of the overburden strata is fairly uniform, this simplification is reasonable [25]. However, surface subsidence is the result of a gradual development of overburden strata from bottom to top after mining, and different compositions of overburden strata have strong impacts on surface subsidence. Although the existing prediction methods take into account the influence of lithology of overburden strata on surface subsidence when choosing the prediction parameters, consideration of overburden remains insufficient [26]. For instance, in China, one of the influence function methods, the probability integral method [14], has been used widely. To study surface subsidence, it regards overburden strata as a granular random medium and classifies overburden strata into three types, hard, medium, and soft, when choosing prediction parameters [14]. When the overburden strata includes UTHS, considering the overburden strata as a homogenous medium is obviously an oversimplification of the overburden condition, which ignores the control function of UTHS on surface subsidence. It does not relate surface subsidence with the movement of UTHS and does not consider the strong influence of the characteristics of movement of UTHS on surface subsidence. Many case studies, such as the movement of thick and hard sandstone in the Datong mine area, the thick glutenite in the Huafeng Coal Mine in Xinwen, and the thick and hard sandstone in the Lutugin Coal Mine in Ukraine, have shown that the control function of UTHS on surface subsidence leads to overall movement of all of the overlying strata up to the ground surface [26]. Considering the previously mentioned shortcomings, the existing prediction methods of subsidence are no longer applicable under the condition of UTHS. Thus, a surface subsidence prediction method for coal mining with the presence of UTHS should be established.

In China, an UTHS is generally defined as a rock stratum that is about hundreds of meters thick [24], with a uniaxial compressive strength of more than 40 MPa [27]. The overburden strata condition of UTHS exists widely in China and other countries. Some examples include the ultrathick conglomerate strata of the Huafeng Coal Mine in China [28], the ultrathick igneous rock of the Haizi Coal Mine in China [24], the ultrathick sandstones of the Tingnan Coal Mine in China, and the ultrathick dolerite sill of the Churcha West Colliery in India [29]. A surface subsidence prediction method for coal mining with the presence of UTHS must consider the control function of UTHS on surface subsidence. To improve the precision of surface subsidence prediction for coal mining with the presence of UTHS, we must know the movement characteristics of UTHS accurately. It should be pointed out that when the thickness of an alluvium layer is more than 100 m, the thick alluvium layer will also have a strong impact on the surface subsidence [30]. Therefore, this paper only considers surface subsidence prediction when the overburden strata have UTHS without a thick alluvium layer.

The existing surface subsidence prediction methods ignore the strong impact and control function of UTHS on surface subsidence. They also lack correct understanding of the movement characteristics of UTHS and do not relate surface subsidence with UTHS movement. Thus, they are not applicable for surface subsidence prediction for coal mining with the presence of UTHS. We conducted actual measurements of surface subsidence attributable to coal mining with the presence of UTHS and established UTHS internal rock movement monitoring drill holes to monitor the UTHS subsidence in the Tingnan Coal Mine. We discovered the relationship between surface subsidence and UTHS movement. We studied the UTHS movement characteristics using Winkler's theory of beams on an elastic foundation, developed a surface subsidence prediction method for coal mining with the presence of UTHS, and evaluated the influences of UTHS thickness, strength, and layer position on surface subsidence. We took the Tingnan Coal Mine as an example and calculated the subsidence curves of strike and dip main sections with different mining dimensions. Then, we predicted the surface subsidence after the mining of the 204, 204 + 205, 204 + 205 + 206, and 204 + 205 + 206 + 207 working surfaces and verified the accuracy of the predicted results using the actual measurement results of surface subsidence of the 204, 204 + 205, and 204 + 205 + 206 working surfaces.

2. Actual Measurement of Surface and UTHS Subsidence for Coal Mines with UTHS

Ignoring the influence of UTHS often leads to distorted prediction results of surface subsidence, as for the previously mentioned Haizi Coal Mine. To study the influence of UTHS on surface subsidence, we conducted long-term surface subsidence measurements at the Tingnan Coal Mine and actual subsidence measurements of the UTHS.

2.1. Surface Subsidence Measurement. The Tingnan Coal Mine is located in the Changwu County, Xianyang, Shaanxi Province, and it has an average mining height of 7.0 m and a coal seam dip angle of 0° in the second panel. There is an ultrathick (222.14 m) and hard sandstone stratum, which is a moderately water-rich aquifer with an average uniaxial compressive strength of 42.2 MPa. The recovery periods of working faces 204, 205, and 206 were November 2011–November 2012, June 2013–November 2014, and January 2015–April 2016, respectively. Currently, the panel is recovering working face 207. Figure 1 shows the layout of the working area in the second panel

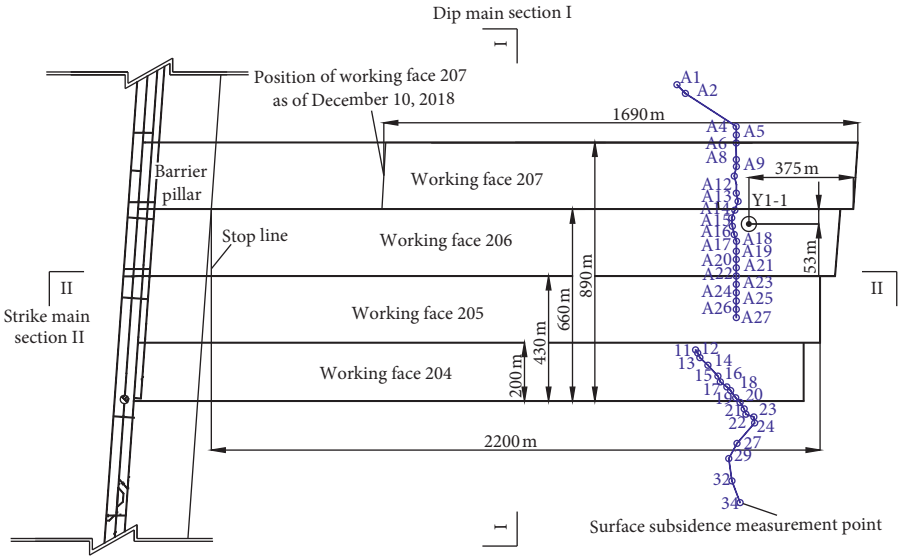

Figure 1: Map of the layout of the working area in the second panel and the positions of surface subsidence measurement points.

and the positions of surface subsidence measurement points, and the integrated stratigraphic column in the second panel can be seen in Figure 2.

Considering the potential influences of the surface landform and streams, a surface subsidence observation line was deployed along the dip of the second panel to observe surface subsidence, as shown in Figure 1. After the mining of the 204, 204 + 205, and 204 + 205 + 206 working surfaces, the measured maximum surface subsidence was 0.248, 1.194, and 1.925 m, respectively. Because of the influence of surface reservoir construction, most of the measurement points could no longer be used to monitor surface subsidence after the recovery of working face 207. Figure 3 shows the observed surface subsidence curves in the dip direction (measurement point no. 34-A1, shown in Figure 1) after the mining of working faces 204, 205, and 206, respectively. Based on the mining experience [14], when the dimensions of the gob in both the strike and dip directions reach 1.2–1.4 times the mining depth of the seam, the surface reaches sufficient mining, which means that when the second panel's mining dimensions in both the strike and dip directions reach 657–766 m, the surface should reach sufficient mining. After the mining of working faces 204, 205, and 206, the strike and dip mining dimensions of the second panel gob were 2200 m and 660 m, respectively. Therefore, the surface of the second panel should have approached sufficient mining. Based on the empirical subsidence coefficient of 0.65 of the Tingnan Coal Mine under sufficient surface mining, after the mining of working faces 204, 205, and 206, the maximum empirical subsidence value should have approached 4.55 m, but the measured maximum surface subsidence value was only 1.925 m, much smaller than 4.55 m, indicating that the surface was far from reaching sufficient mining. Under the UTHS condition, the required dimensions of the gob in the strike and dip directions are much greater than 1.2–1.4 times the mining depth in the seam. In addition, the predicted surface subsidence curves of the observation line were also plotted using the influence function method [14] with empirical parameters collated from the Tingnan Coal Mine. The maximum values of the predicted surface subsidence are 2.4, 3.71, and 4.07 m, respectively (Figure 3). The influence function method calculations produced results significantly larger than those obtained by measurements. Based on the above results, we could be certain that UTHS has a strong impact on surface subsidence.

2.2. Measurement of UTHS Subsidence. As the UTHS is inside the overburden, it is impossible to measure its exact amount of deflection. After the mining of working face 206, to monitor the relative movement between the UTHS and the surface during the mining of working face 207, we drilled a strata displacement-monitoring borehole Y1-1 inside the overburden strata of working face 206. The position of the borehole is shown in Figure 1, and no separation spaces were detected during drill work. The measuring point was placed 130 m below the UTHS top boundary and connected to a surface displacement recorder using a wire rope to monitor the relative movement between the measuring point and the surface, as shown in Figure 2 and Figures 4(a) and 4(b). As of September 3, 2018, working face 207 had been mined 916.8 m past the monitoring borehole. The surface of Y1-1 had subsided another 1.352 m since the mining of working face 207 and was still subsiding at 0.41 mm per day without showing signs of becoming stable. However, the measuring point inside the UTHS on the other side subsided only 0.077 m and had already stabilized. The monitoring results are shown in Figure 4(c). Evidently, the UTHS and the overburden strata up to the surface have approximately made an overall movement, and the UTHS subsidence can approximately represent the surface subsidence.

	No.	Thickness (m)	Depth (m)	Lithology	Stratigraphic column	
	34	35.40	35.40	Loess		
	33	29.60	65.00	Coarse sandstone		
	32	14.85	79.85	Sandy mudstone		
	31	1.35	81.2	Fine sandstone		
	30	5.75	86.95	Sandy mudstone		
	29	0.85	87.8	Fine sandstone		
	28	5.95	93.75	Sandy mudstone		
	27	6.00	99.75	Coarse sandstone gravel		
	26	22.89	122.64	Coarse sandstone		
	25	37.77	160.41	Conglomerate		
	24	6.54	166.95	Coarse sandstone gravel		
Measuring point (296.95 m)	23	222.14	389.09	Coarse sandstone		UTHS
	22	3.05	392.14	Conglomerate		
	21	8.50	400.64	Medium sandstone		
	20	25.90	426.54	Conglomerate		
	19	10.53	437.07	Sandy mudstone		
	18	3.13	440.20	Coarse sandstone		
	17	17.13	457.33	Sandy mudstone		
	16	3.45	460.78	Coarse sandstone		
	15	11.63	472.41	Sandy mudstone		
	14	8.00	480.41	Coarse sandstone gravel		
	13	4.70	485.11	Fine sandstone		
	12	3.55	488.66	Mudstone		
	11	8.14	496.80	Siltstone		
	10	1.50	498.30	Coarse sandstone		
	9	1.32	499.62	Mudstone		
	8	0.20	499.82	Coal seam		
	7	1.90	501.72	Mudstone		
	6	2.13	503.85	Medium sandstone		
	5	12.00	515.85	Sandy mudstone		
	4	8.70	524.55	Fine sandstone		
	3	6.46	531.01	Coarse sandstone		
	2	1.21	532.22	Mudstone		
	1	15.03	547.25	Coal seam		

Figure 2: The integrated stratigraphic column in the second panel.

The measured surface and UTHS subsidence at the Tingnan Coal Mine show that UTHS has a strong impact on the surface subsidence. Thus, the lack of a correct understanding of the surface subsidence rules caused by UTHS movement in different mining dimensions could lead to a distorted prediction result of surface subsidence. As a possible solution, we could take the subsidence of UTHS as an approximate surface subsidence and then predict the surface subsidence by calculating the UTHS subsidence. In this paper, the UTHS subsidence represents the surface subsidence.

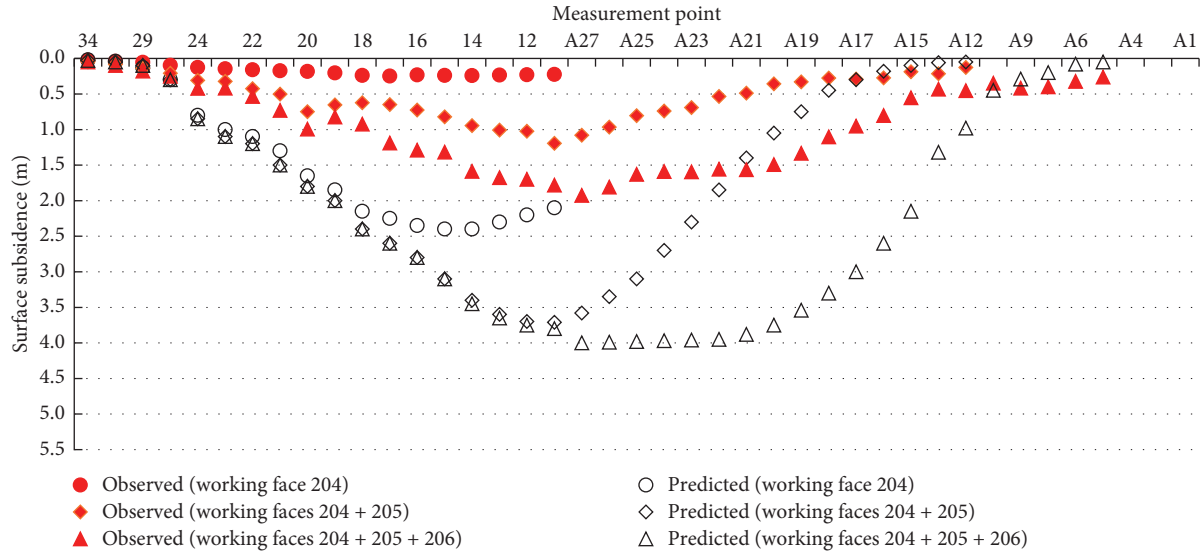

Figure 3: Comparison between the measured subsidence value and the predicted subsidence value by the probability integral method at the surface subsidence measurement point (measurement point no. 34-A1).

3. Surface Subsidence Prediction Method for Coal Mining with UTHS

3.1. Mechanical Model for Subsidence Prediction for Coal Mining with UTHS. After a coal seam is mined, a breaking movement and a flexural subsidence are expected in the overburden strata of the mining site, which is composed of the caved zone, fractured zone, and continuous deformation zone [12, 26]. The UTHS, which is generally in the continuous deformation zone, is subject to a curve subsidence rather than a breaking movement [12, 26]. To simplify the process, we consider the goaf to be filled up with bulked rocks from the caved and fractured zones [31]; the rocks underlying the UTHS are considered as an elastic foundation complying with the Winkler elastic foundation hypothesis [31–36]. The UTHS is then thought of as an elastic foundation beam on which both the dead weight of the UTHS itself and its load act as uniform loads [31–35], and it has a dip angle of 0°. In Chinese coal mines, the most commonly used mining method is longwall mining in which the stoping space created by the stoping of one or more working faces is rectangular in shape, and the mining area contains two main sections: the dip main section I and the strike main section II. For each of the two main sections, based on the aforementioned assumptions, we established a mechanical model for subsidence prediction for the coal mining with the presence of UTHS, as shown in Figure 5.

The symbol q (MPa) represents the weight of the UTHS and the strata on it. Furthermore, H (m) is the thickness of the UTHS, E (GPa) is the elastic modulus of the UTHS, I (m^4) is the inertia moment of the UTHS, L_1 (m) is the mining dimension of main section I, L_2 (m) is the mining dimension of main section II, k (N/m^3) is the foundation coefficient of the UTHS at the coal side, k_c (N/m^3) is the foundation coefficient of the UTHS at the goaf side, p_s (MPa) is the foundation reaction of the UTHS at the coal side, and p_c (MPa) is the foundation reaction at the goaf side.

If the calculated main section in Figure 5(b) is main section I, we assume that main section II has reached sufficient mining. As the UTHS in Figure 5(b) is symmetric about $x = L_1/2$, only half of the UTHS was used for our analysis, as shown in Figure 5(c). The differential equations of the deflection curves can be established for the UTHS as follows:

$$\mathrm{EI}\frac{d^4 w_{\mathrm{Is}}(x)}{dx^4} + kbw_{\mathrm{Is}}(x) = qb, \quad x \le 0, \tag{1}$$

$$\mathrm{EI}\frac{d^4 w_{\mathrm{Ic}}(x)}{dx^4} + k_c bw_{\mathrm{Ic}}(x) = qb, \quad 0 \le x \le \frac{L_1}{2}. \tag{2}$$

In the equation, $w_{\mathrm{Is}}(x)$ (m) and $w_{\mathrm{Ic}}(x)$ (m) are the UTHS deflection curve equations of main section I at the coal side and the goaf side, respectively, I (m^4) is the moment of inertia of the UTHS, where $I = bH^3/12$, and b (m) is the width of the beam, considered to be equal to unity, i.e., $b = 1$.

Then, the general solution for equation (1) is

$$w_{\mathrm{Is}}(x) = C_{\mathrm{I1}}e^{a_{\mathrm{I1}}x}\cos(a_{\mathrm{I1}}x) + C_{\mathrm{I2}}e^{a_{\mathrm{I1}}x}\sin(a_{\mathrm{I1}}x) + C_{\mathrm{I3}}e^{-a_{\mathrm{I1}}x}\cos(a_{\mathrm{I1}}x) + C_{\mathrm{I4}}e^{-a_{\mathrm{I1}}x}\sin(a_{\mathrm{I1}}x) + \frac{q}{k}. \tag{3}$$

In the equation, $a_{\mathrm{I1}} = \sqrt[4]{k/4\mathrm{EI}}$.

As $x \longrightarrow -\infty$ and $w_{\mathrm{Is}}(x) \longrightarrow q/k$, these conditions can only be satisfied when C_{I3} and C_{I4} are equal to zero. Additionally, because q/k in equation (3) is caused by the premining compression of the seam, the UTHS deflection

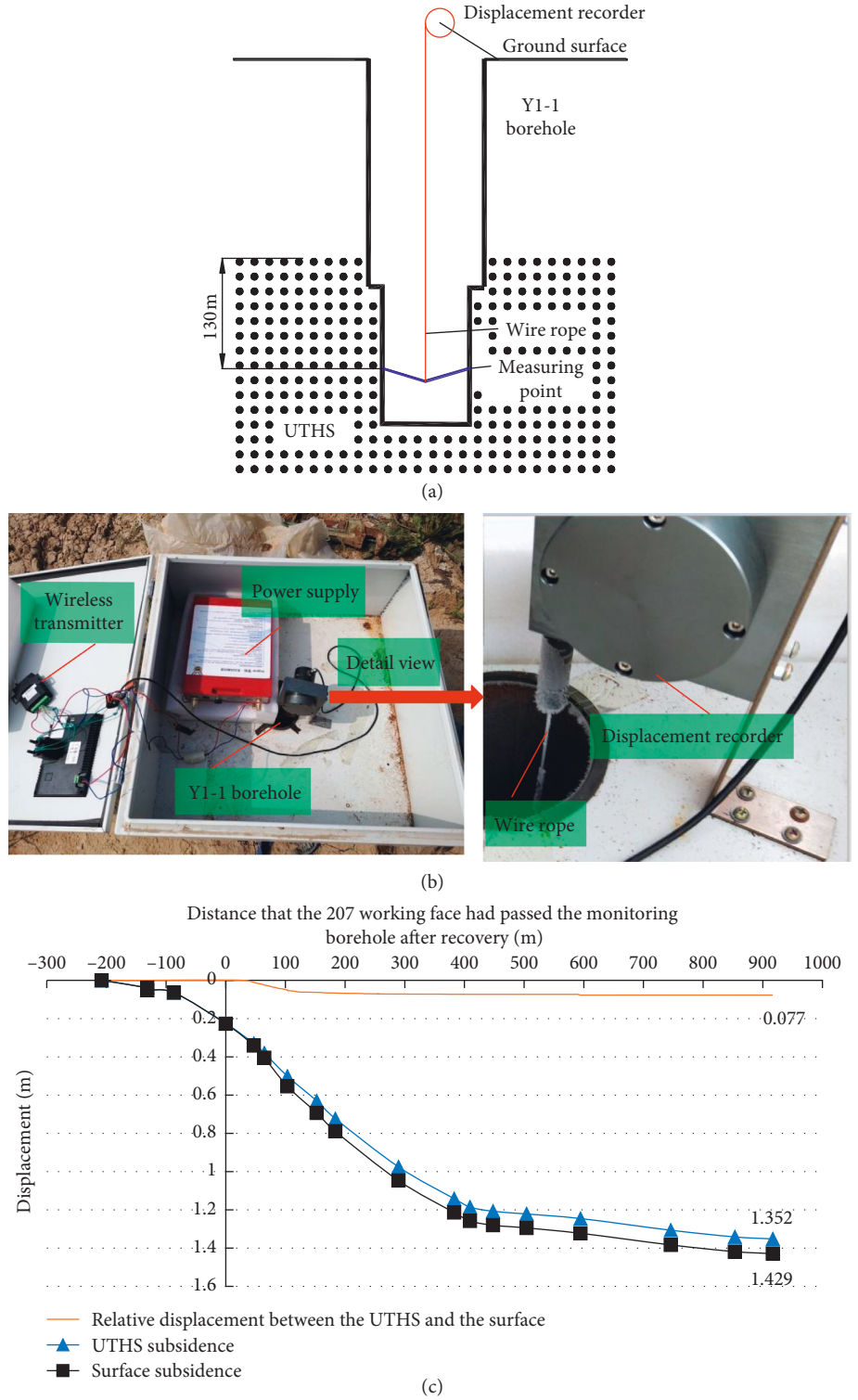

Figure 4: Subsidence monitoring of surface and UTHS after recovery of the 207 working face. (a) Schematic diagram of UTHS subsidence monitoring drill hole. (b) UTHS subsidence monitoring equipment. (c) UTHS and surface subsidence curves.

curve equation at the coal side induced by coal mining, $w_{Iw}(x)$, is equal to

$$w_{Iw}(x) = C_{I1}e^{a_{I1}x}\cos(a_{I1}x) + C_{I2}e^{a_{I1}x}\sin(a_{I1}x). \quad (4)$$

Then, the general solution for equation (2) is

$$w_{Ic}(x) = C_{I5}e^{a_{I2}x}\cos(a_{I2}x) + C_{I6}e^{a_{I2}x}\sin(a_{I2}x) + C_{I7}e^{-a_{I2}x}\cos(a_{I2}x) + C_{I8}e^{-a_{I2}x}\sin(a_{I2}x) + \frac{q}{k_c}. \quad (5)$$

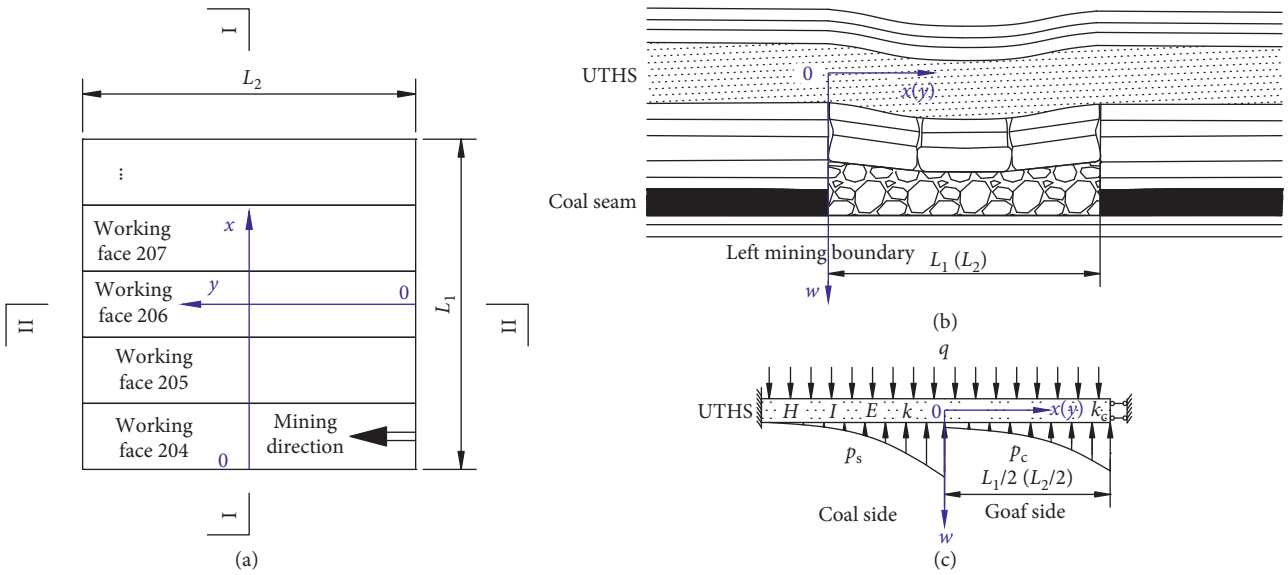

Figure 5: Mechanical model for subsidence prediction for coal mining with UTHS. (a) Simplified floor plan of working faces of second panel in Tingnan Coal Mine. (b) Cross section plot of overburden strata with UTHS in the main section I (II). (c) Subsidence prediction mechanical model for coal mining with presence of UTHS in the main section I (II).

In the equation, $a_{I2} = \sqrt[4]{k_c/4EI}$.

The UTHS deflection curve equation at the goaf side, $w_{Ic}(x)$, is shown in equation (5). From the relationship among the rotation angle, bending moment, and shear force of the UTHS with its deflection curve equation in equation (6) [32, 34, 36], by substituting the deflection curve equations (4) and (5) into (6), we can derive the rotation angle $\theta_{Iw}(x)$, bending moment $M_{Iw}(x)$, and shear force $Q_{Iw}(x)$ of the UTHS at the coal side as well as the rotation angle $\theta_{Ic}(x)$, bending moment $M_{Ic}(x)$, and shear force $Q_{Ic}(x)$ of the UTHS at the goaf side.

$$\begin{cases} \theta(x) = \dfrac{dw(x)}{dx}, \\ M(x) = -\mathrm{EI}\dfrac{dw^2(x)}{dx^2}, \\ Q(x) = -\mathrm{EI}\dfrac{dw^3(x)}{dx^3}. \end{cases} \tag{6}$$

The deflection curve equations (4) and (5) contain six unknown parameters: C_{I1}, C_{I2}, C_{I5}, C_{I6}, C_{I7}, and C_{I8}. The UTHS is continuous at $x = 0$, where the subsidence, rotation angle, bending moment, and shear force of the UTHS are equal. The model is symmetric about $x = L_1/2$, where the shear force and rotation angle of the UTHS are equal to zero [34, 36]. Using these continuity and boundary conditions for the UTHS in equation (7), we can derive the six unknown parameters. By substituting those values into equations (4) and (5), we obtain the UTHS deflection curve equations at the coal side and the goaf side.

$$\begin{cases} \left.\begin{array}{l} w_{Iw}(0) = w_{Ic}(0) \\ \theta_{Iw}(0) = \theta_{Ic}(0) \\ Q_{Iw}(0) = Q_{Ic}(0) \\ M_{Iw}(0) = M_{Ic}(0) \end{array}\right\} \text{continuity conditions,} \\ \left.\begin{array}{l} \theta_{Ic}\left(\dfrac{L_1}{2}\right) = 0 \\ Q_{Ic}\left(\dfrac{L_1}{2}\right) = 0 \end{array}\right\} \text{boundary conditions.} \end{cases} \tag{7}$$

When $w_{Ic}(L_0/2) = W_{max}$, i.e., when the mining width L_1 is equal to L_0, the UTHS will be under sufficient mining and the maximum subsidence [14, 27] of the UTHS reaches the maximum W_{max} under this geological mining condition.

$$W_{max} = \delta M. \tag{8}$$

The symbol δ represents the subsidence coefficient [14, 27], which can be found in the literatures [14, 27], whereas M is the mining thickness of the seam.

When $L_1 \le L_0$, the unknown values of C_{I1}, C_{I2}, C_{I5}, C_{I6}, C_{I7}, and C_{I8} in $w_{Iw}(x)$ and $w_{Ic}(x)$ are determined by equation (7); as L_1 increases, these parameters will also change, i.e., the maximum subsidence of the UTHS will change with the increase of L_1. Then, when main section II reaches sufficient mining and main section I does not, the UTHS deflection curve equation of main section I can be written as follows:

$$\begin{cases} w_{\mathrm{Iw}}(x) = C_{\mathrm{I1}}e^{a_{\mathrm{I1}}x}\cos(a_{\mathrm{I1}}x) + C_{\mathrm{I2}}e^{a_{\mathrm{I1}}x}\sin(a_{\mathrm{I1}}x), & x \le 0, \\ w_{\mathrm{Ic}}(x) = C_{\mathrm{I5}}e^{a_{\mathrm{I2}}x}\cos(a_{\mathrm{I2}}x) + C_{\mathrm{I6}}e^{a_{\mathrm{I2}}x}\sin(a_{\mathrm{I2}}x) + C_{\mathrm{I7}}e^{-a_{\mathrm{I2}}x}\cos(a_{\mathrm{I2}}x) + C_{\mathrm{I8}}e^{-a_{\mathrm{I2}}x}\sin(a_{\mathrm{I2}}x) + \dfrac{q}{k_{\mathrm{c}}}, & 0 \le x \le \dfrac{L_1}{2}. \end{cases} \tag{9}$$

When $L_1 > L_0$, to determine the six unknown parameters C_{I1}, C_{I2}, C_{I5}, C_{I6}, C_{I7}, and C_{I8} in $w_{\mathrm{Iw}}(x)$ and $w_{\mathrm{Ic}}(x)$, the continuity conditions in equation (7) remain the same at $x = 0$, but the boundary conditions change to $\theta_{\mathrm{c}}(L_0/2) = 0$ and $Q_{\mathrm{c}}(L_0/2) = 0$. These unknown values will no longer vary with the increase of L_1. Thus, the maximum subsidence of the UTHS will not vary with the increase of L_1. Then, when both main section I and main section II reach sufficient mining, the UTHS deflection curve equation of main section I is

$$\begin{cases} w_{\mathrm{Iw}}(x) = C_{\mathrm{I1}}e^{a_{\mathrm{I1}}x}\cos(a_{\mathrm{I1}}x) + C_{\mathrm{I2}}e^{a_{\mathrm{I1}}x}\sin(a_{\mathrm{I1}}x), & x \le 0, \\ w_{\mathrm{Ic}}(x) = C_{\mathrm{I5}}e^{a_{\mathrm{I2}}x}\cos(a_{\mathrm{I2}}x) + C_{\mathrm{I6}}e^{a_{\mathrm{I2}}x}\sin(a_{\mathrm{I2}}x) + C_{\mathrm{I7}}e^{-a_{\mathrm{I2}}x}\cos(a_{\mathrm{I2}}x) + C_{\mathrm{I8}}e^{-a_{\mathrm{I2}}x}\sin(a_{\mathrm{I2}}x) + \dfrac{q}{k_{\mathrm{c}}}, & 0 \le x \le \dfrac{L_0}{2}, \\ w_{\mathrm{Ic}}(x) = W_{\max}, & \dfrac{L_0}{2} \le x \le \dfrac{L_1}{2}. \end{cases} \tag{10}$$

If the calculated main section in Figure 5(b) is main section II, we assume that main section I has reached sufficient mining. In the same way, if we replace the parameters of main section I (x, L_1, $w_{\mathrm{Is}}(x)$, $w_{\mathrm{Ic}}(x)$, $w_{\mathrm{Iw}}(x)$, a_{I1}, a_{I2}, C_{I1}, C_{I2}, C_{I3}, C_{I4}, C_{I5}, C_{I6}, C_{I7}, C_{I8}, $\theta_{\mathrm{Iw}}(x)$, $M_{\mathrm{Iw}}(x)$, $Q_{\mathrm{Iw}}(x)$, $\theta_{\mathrm{Ic}}(x)$, $M_{\mathrm{Ic}}(x)$, and $Q_{\mathrm{Ic}}(x)$) with the parameters of main section II (y, L_2, $w_{\mathrm{IIs}}(y)$, $w_{\mathrm{IIc}}(y)$, $w_{\mathrm{IIw}}(y)$, a_{II1}, a_{II2}, C_{II1}, C_{II2}, C_{II3}, C_{II4}, C_{II5}, C_{II6}, C_{II7}, C_{II8}, $\theta_{\mathrm{IIw}}(y)$, $M_{\mathrm{IIw}}(y)$, $Q_{\mathrm{IIw}}(y)$, $\theta_{\mathrm{IIc}}(y)$, $M_{\mathrm{IIc}}(y)$, and $Q_{\mathrm{IIc}}(y)$) in the calculation, we can obtain the deflection curve equation of section II with UTHS when main section I reaches sufficient mining and main section II does not:

$$\begin{cases} w_{\mathrm{IIw}}(y) = C_{\mathrm{II1}}e^{a_{\mathrm{II1}}y}\cos(a_{\mathrm{II1}}y) + C_{\mathrm{II2}}e^{a_{\mathrm{II1}}y}\sin(a_{\mathrm{II1}}y), & y \le 0, \\ w_{\mathrm{IIc}}(y) = C_{\mathrm{II5}}e^{a_{\mathrm{II1}}y}\cos(a_{\mathrm{II2}}y) + C_{\mathrm{II6}}e^{a_{\mathrm{II2}}y}\sin(a_{\mathrm{II2}}y) + C_{\mathrm{II7}}e^{-a_{\mathrm{II2}}y}\cos(a_{\mathrm{II2}}y) + C_{\mathrm{II8}}e^{-a_{\mathrm{II2}}y}\sin(a_{\mathrm{II2}}y) + \dfrac{q}{k_{\mathrm{c}}}, & 0 \le y \le \dfrac{L_2}{2}. \end{cases} \tag{11}$$

When both main section I and main section II reach sufficient mining, the UTHS deflection curve equation of main section II is

$$\begin{cases} w_{\mathrm{IIw}}(y) = C_{\mathrm{II1}}e^{a_{\mathrm{II1}}y}\cos(a_{\mathrm{II1}}y) + C_{\mathrm{II2}}e^{a_{\mathrm{II1}}y}\sin(a_{\mathrm{II1}}y), & y \le 0, \\ w_{\mathrm{IIc}}(y) = C_{\mathrm{II5}}e^{a_{\mathrm{II2}}y}\cos(a_{\mathrm{II2}}y) + C_{\mathrm{II6}}e^{a_{\mathrm{II2}}y}\sin(a_{\mathrm{II2}}y) + C_{\mathrm{II7}}e^{-a_{\mathrm{II2}}x}\cos(a_{\mathrm{II2}}y) + C_{\mathrm{II8}}e^{-a_{\mathrm{II2}}y}\sin(a_{\mathrm{II2}}y) + \dfrac{q}{k_{\mathrm{c}}}, & 0 \le y \le \dfrac{L_0}{2}, \\ w_{\mathrm{IIc}}(y) = W_{\max}, & \dfrac{L_0}{2} \le y \le \dfrac{L_2}{2}, \end{cases} \tag{12}$$

where $w_{\mathrm{IIw}}(y)$ (m) is the UTHS deflection curve equation of main section II at the coal side, and $w_{\mathrm{IIc}}(y)$ (m) is the UTHS deflection equation of main section II at the gob side.

To solve the above equations, it is necessary to determine the parameters E, H, M, L_1, L_2, q, k, and k_{c}. The first five of these (E, H, M, L_1, and L_2) can be determined in relation to

the borehole columns, the physical-mechanical parameter test results, and the actual mining conditions. The uniform load on the UTHS, q, can be calculated as [26]

$$q = \sum_{j=1}^{z} \gamma_j h_j. \tag{13}$$

Here, h_j is the thickness of the UTHS and any of the overburden load strata, γ_j is the bulk density of the UTHS and any of the overburden load strata, and z is the total number of the UTHS and the overburden load strata.

The foundation coefficient k of the UTHS at the coal side is calculated as [21, 35, 36]

$$k = \frac{1}{\sum_{i=1}^{n} H_i/E_i}. \tag{14}$$

The variable H_i represents the thickness of any of the foundation strata, E_i is the elastic modulus of any of the foundation strata, and n is the total number of the foundation strata, often taken as the total number of strata between the UTHS and the thick and hard rock stratum in the coal floor.

Because the model assumes that the fractured rock in the gob region satisfies Winkler's elastic foundation hypothesis, we can calculate the ground coefficient k_c of UTHS at the gob side if we know the subsidence value [36] of UTHS and the corresponding load bearing of the foundation [36] in the gob region. When the surface reaches sufficient mining, UTHS subsidence reaches the maximum value W_{max} under this mining condition [14], and the corresponding load bearing of the foundation at the gob side is q [26]. Then, the ground coefficient in the gob region k_c can be written as

$$k_c = \frac{q}{W_{max}}. \tag{15}$$

3.2. Subsidence Prediction Equation of Main Sections. According to the actual mining dimensions of the two main sections, the surface has four mining extents [14]: main section I does not reach sufficient mining, but main section II does; main section I reaches sufficient mining, but main section II does not; both main section I and main section II reach sufficient mining; and neither of the main sections reaches sufficient mining.

(1) When main section I does not reach sufficient mining but main section II does, equation (9) is the UTHS deflection curve equation of main section I. The UTHS deflection curve equation of main section II can be calculated through equation (12), but the equation needs to be multiplied by a coefficient, λ_I, which is named the mining extent coefficient [14] of main section I and represents the times of reduction of the main section II subsidence value when main section I is at different levels of insufficient mining rather than sufficient mining.

$$\lambda_I = \frac{w_{Ic}(L_1/2)}{W_{max}}, \tag{16}$$

$w_{Ic}(L_1/2)$ is the subsidence value of the point with the coordinate of $L_1/2$ on main section I when main section II is under sufficient mining, and it is calculated through equation (9).

(2) When main section II does not reach sufficient mining but main section I does, equation (11) is the UTHS deflection curve equation of main section II. The UTHS deflection curve equation of main section I can be calculated through equation (10), but the equation needs to be multiplied by a coefficient, λ_{II}, which is named the mining extent coefficient [14] of main section II and represents the times of reduction of the main section I subsidence value when main section II is at different levels of insufficient mining rather than sufficient mining.

$$\lambda_{II} = \frac{w_{IIc}(L_2/2)}{W_{max}}, \tag{17}$$

$w_{IIc}(L_2/2)$ is the subsidence value of the point with the coordinate of $L_2/2$ on main section II when main section I is under sufficient mining, and it is calculated through equation (11).

(3) When both main section I and main section II reach sufficient mining, the UTHS deflection curve equations of main section I and main section II are equations (10) and (12), respectively.

(4) When neither of them reaches sufficient mining, the UTHS deflection curve equation of main section I can still be calculated through equation (9), but the equation needs to be multiplied by a coefficient, λ_{II}, which is shown in equation (17). The subsidence of main section II can still be calculated through equation (11), but this equation also needs to be multiplied by a coefficient, λ_I, which is shown in equation (16).

3.3. Subsidence Prediction Equation on Any Arbitrary Cross Section Parallel to the Main Sections. Section 3.2 solves the subsidence prediction equations of the two main sections under four mining extents in the mining area. The subsidence distributions parallel to the cross sections of main section I and main section II are similar to those of the corresponding main sections [14], but the values are smaller than the predicted subsidence values of the main sections obtained in Section 3.2. The magnitudes are ζ_{II} times the deflection curve equation of main section I and ζ_I times the deflection curve equation of main section II in Section 3.2, respectively. Therefore, if the cross section parallel to main section I is $y = y_0$ and the cross section parallel to main section II is $x = x_0$, we have the following expression:

$$\begin{cases} \zeta_{II} = \dfrac{w_{IIw}(y_0)}{w_{IIc}(L_2/2)}, & y_0 \le 0, \\ \zeta_{II} = \dfrac{w_{IIc}(y_0)}{w_{IIc}(L_2/2)}, & 0 \le y_0 \le \dfrac{L_2}{2}. \end{cases} \tag{18}$$

In the equation, $w_{\mathrm{IIw}}(y_0)$ and $w_{\mathrm{IIc}}(y_0)$ are the subsidence values of point y_0 on main section II when main section I has reached sufficient mining. When main section II has not reached sufficient mining, $w_{\mathrm{IIw}}(y_0)$ and $w_{\mathrm{IIc}}(y_0)$ can be calculated through equation (11); when main section II has reached sufficient mining, $w_{\mathrm{IIw}}(y_0)$ and $w_{\mathrm{IIc}}(y_0)$ can be calculated through equation (12).

$$\begin{cases} \zeta_{\mathrm{I}} = \dfrac{w_{\mathrm{Iw}}(x_0)}{w_{\mathrm{Ic}}(L_1/2)}, & x_0 \le 0, \\ \zeta_{\mathrm{I}} = \dfrac{w_{\mathrm{Ic}}(x_0)}{w_{\mathrm{Ic}}(L_1/2)}, & 0 \le x_0 \le \dfrac{L_1}{2}. \end{cases} \tag{19}$$

In the equation, $w_{\mathrm{Iw}}(x_0)$ and $w_{\mathrm{Ic}}(x_0)$ are the subsidence values of point x_0 on main section I when main section II has reached sufficient mining. When main section I has not reached sufficient mining, $w_{\mathrm{Iw}}(x_0)$ and $w_{\mathrm{Ic}}(x_0)$ can be calculated through equation (9); when main section I has reached sufficient mining, $w_{\mathrm{Iw}}(x_0)$ and $w_{\mathrm{Ic}}(x_0)$ can be calculated through equation (10).

After solving the subsidence prediction equation on any arbitrary cross section parallel to the main sections, we can predict the subsidence of the whole mining area.

4. Example of Calculation and Verification Using the Proposed Surface Subsidence Prediction Method

4.1. Example of Surface Subsidence Calculation for the Tingnan Coal Mine. The model calculation parameters, as shown in Table 1, were chosen according to the geological mining conditions of the second panel in Tingnan Coal Mine, the rock mechanical parameter test results, and the model parameter determination method described in Section 3.1.

To calculate the surface subsidence under different mining dimensions L_1 of main section I, we considered that with the increase of mining number on the working face of the second panel, the mining dimension L_1 of main section I increases. The average propelling distance of main section II is approximately 2200 m. We took $L_2 = 2200$ m and calculated according to the calculation method in Section 3.1. The calculation result indicates that main section II has reached sufficient mining. For main section I, we took $L_1 = 200$ m (working face 204), 430 m (working faces 204 + 205), 660 m (working faces 204 + 205 + 206), 890 m (working faces 204 + 205 + 206 + 207), 1120 m, 1350 m, and 1580 m. According to the calculation method in Section 3 and the symmetric nature of the mechanical model, the subsidence curves of main section I when taking different mining dimensions L_1 are shown in Figure 6.

To calculate the surface subsidence of main section I when the mining dimension L_1 of main section I is 200 m, 430 m, 660 m, 890 m, 1120 m, 1350 m, and 1580 m, with increase of L_1, main section I changes from insufficient mining to sufficient mining. According to the calculation methods in Section 3 and the symmetric nature of the mechanical model, the subsidence curves of main section II when taking different mining dimensions L_1 are shown in Figure 7.

Table 1: The model calculation parameters in the Tingnan Coal Mine.

E (GPa)	k (MN/m^3)	k_c (MN/m^3)	q (MPa)	H (m)	δ	M (m)
11.5	19	2.28	10.37	222.14	0.65	7

From Figures 6 and 7, when $L_1 = L_2 = L_0 = 1350$ m, both main section I and main section II reach sufficient mining, and the maximum subsidence value reaches the maximum value $W_{\max}$ of 4.55 m. When $L_1 \le L_0$, with increase of L_1, the maximum subsidence value increases gradually. When $L_1 > L_0$, with increase of L_1, the maximum subsidence value does not change further. Thus, under the UTHS mining condition in the Tingnan Coal Mine, the required dimension (1350 m) in the strike and dip directions in the gob region when the surface reaches sufficient mining is much larger than the empirical value (1.2–1.4 times the seam mining depth of 657–766 m), which verifies the actual measurement results in Section 2.1.

The calculated subsidence curves of main section I and main section II under different mining dimensions L_1 of main section I can be used in the calculation method in Section 3.3 to solve the subsidence prediction equation for any arbitrary cross section parallel to the main sections, and then the subsidence of the whole mining area can be predicted. Figure 8 shows the subsidence contour maps after the mining of working faces 204, 205, 206, and 207 calculated by the proposed prediction method, respectively.

4.2. Verification of Actual Measurement of Surface Subsidence in the Tingnan Coal Mine. The subsidence at each measurement point in Figure 1 after the recovery of working faces 204, 205, and 206, respectively, can be obtained by the proposed prediction method, and comparing these values with the measured subsidence values can verify the correctness of the proposed prediction method. The predicted subsidence at each point can be obtained from Figure 8, and the comparison between the predicted and measured results is shown in Figure 9. As indicated by the figure, the predicted results are consistent with the measured results, which proves the correctness of the proposed prediction method.

5. Discussion

We investigated the influences of UTHS thickness, strength, and layer position changes on the surface subsidence of main section I when main section II of the Tingnan Coal Mine reaches sufficient mining with the mining dimension of main section I of $L_1 = 660$ m using the proposed prediction method. In the calculation parameters in Table 1, by prescribing UTHS thickness H as 100 m, 160 m, 222 m, and 300 m, respectively, or strength E as 11.5 GPa, 19.5 GPa, 27.5 GPa, and 35.5 GPa, respectively, we calculated surface subsidence with different H or E to show the influences of UTHS thickness and strength on surface subsidence. The

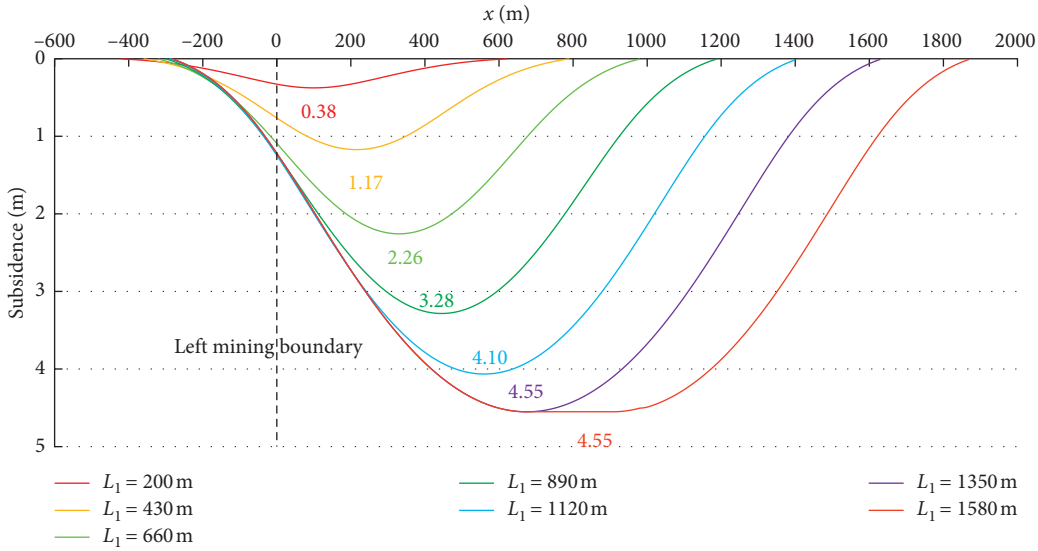

Figure 6: Subsidence curves of main section I when taking different mining dimensions L_1.

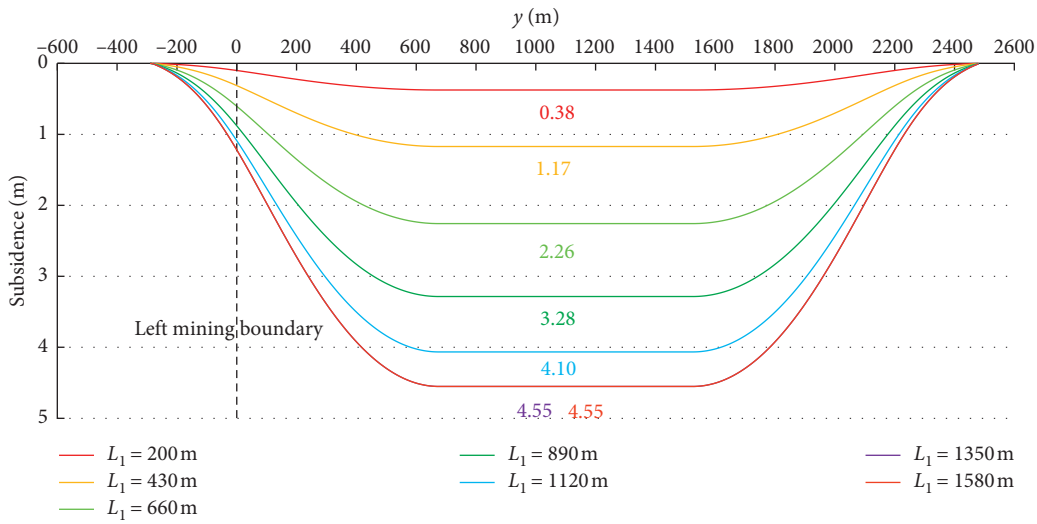

Figure 7: Subsidence curves of main section II when taking different mining dimensions of main section I.

calculated results are shown in Figure 10. As shown in Figures 10(a) and 10(b), with increase of UTHS thickness or strength, the range of surface subsidence increases significantly and the maximum surface subsidence value decreases significantly. Figure 10(c) shows the surface subsidence prediction results after moving the UTHS by +131.55 m, +67.2 m, 0, and −51.55 m, respectively. It represents the influences of different layer positions on the surface subsidence. From Figure 10(c), we can determine that when the distance between UTHS and the seam increases, the maximum surface subsidence value decreases significantly and the range of surface subsidence increases slightly. Comparing Figures 10(a)–10(c), it can be seen that there are significant differences in surface subsidence curves under different UTHS thicknesses, strengths, and layer positions. Thus, different overburden strata compositions have a strong impact on the distribution of surface subsidence.

6. Conclusions

UTHS has a strong impact on the distribution of surface subsidence, but current surface subsidence prediction methods lack consideration of the influence of UTHS on surface subsidence. These methods ignore the control function on surface subsidence of UTHS. Furthermore, they do not appropriately consider the movement characteristics of UTHS and do not relate surface subsidence attributable to coal mining with the presence of UTHS. Therefore, our paper describes a surface subsidence prediction method for coal mining with the presence of UTHS. The results obtained are summarized below.

In our study, actual measurements of surface subsidence for coal mining with UTHS were conducted, and UTHS internal rock movement monitoring drill holes were established to monitor the subsidence of UTHS in the

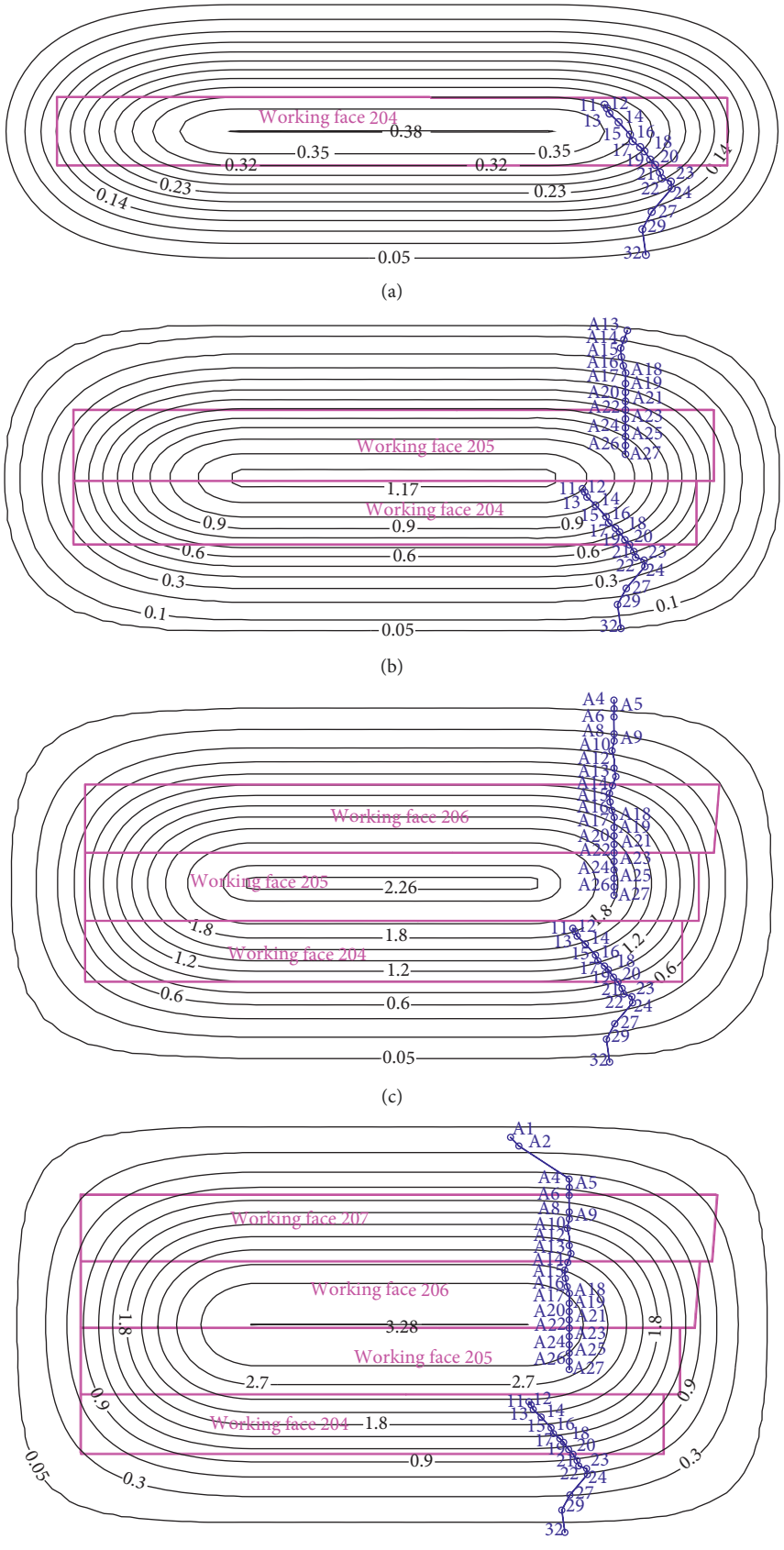

Figure 8: Subsidence contour maps after the mining of working faces 204, 205, 206, and 207, respectively, in the second panel. (a) After the mining of working face 204. (b) After the mining of working faces 204 and 205. (c) After the mining of working faces 204, 205, and 206. (d) After the mining of working faces 204, 205, 206, and 207.

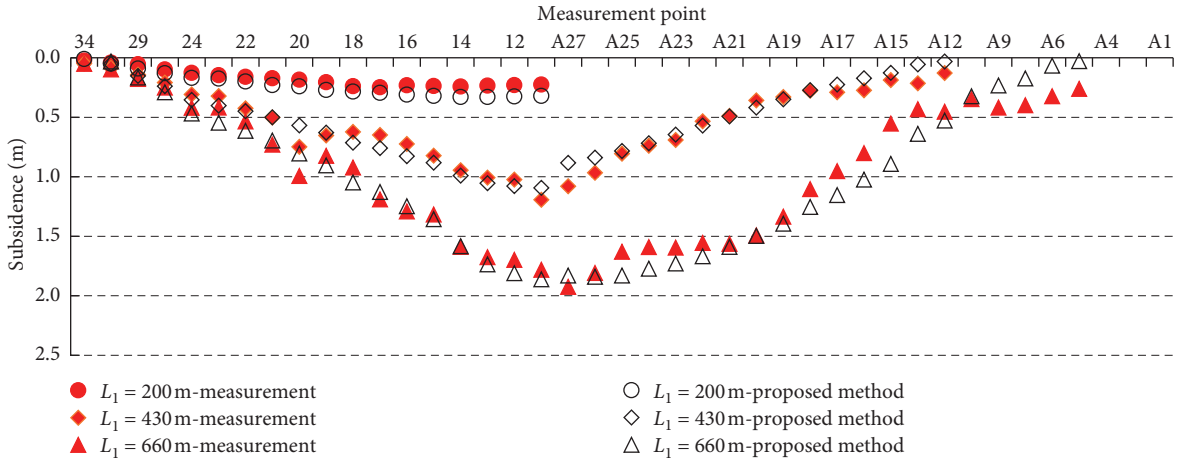

FIGURE 9: Comparison between predicted results obtained by the proposed method and measured results at the measurement points of surface subsidence.

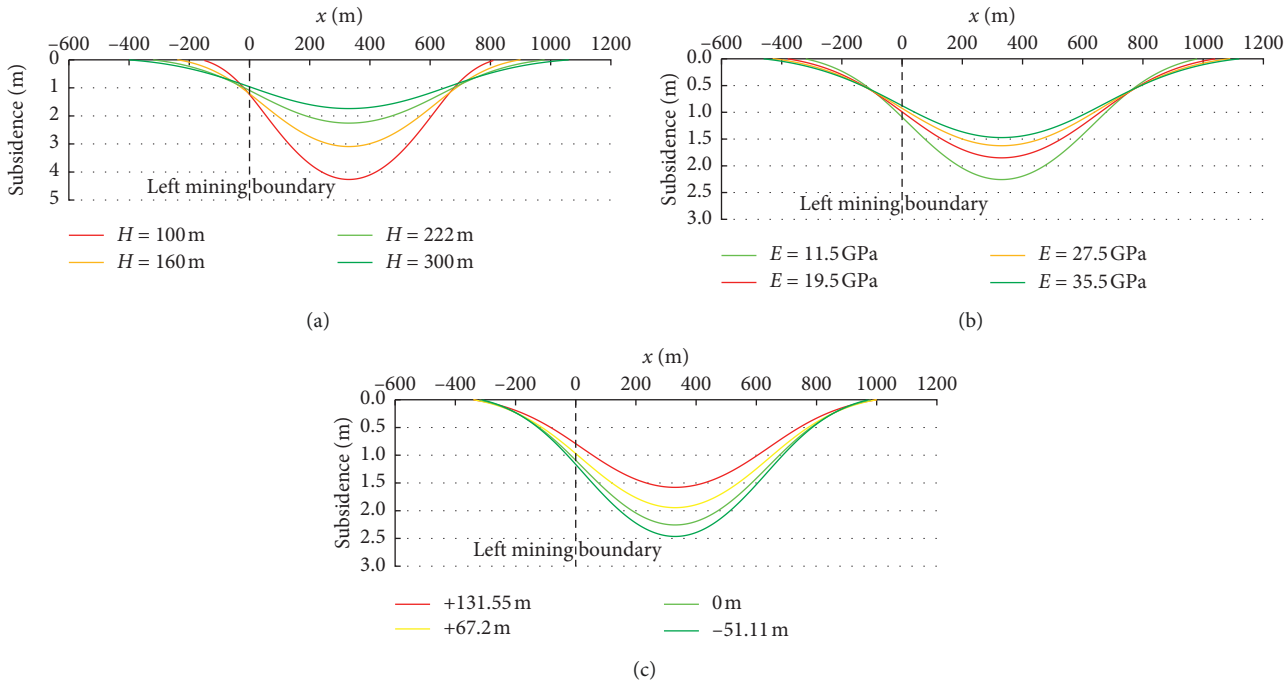

FIGURE 10: Subsidence curves of main section I with different overburden strata compositions. (a) Different UTHS thicknesses. (b) Different UTHS strengths. (c) Different UTHS positions.

Tingnan Coal Mine. It was found that there was a relationship between surface subsidence and UTHS movement. The results showed that under the UTHS mining condition, the required dimension in the strike and dip directions in the gob region is much larger than the empirical value when the surface reaches sufficient mining and that the actual measured value of surface subsidence is much smaller than the empirical value. The subsidence of UTHS is approximately equal to the surface subsidence. The movement of UTHS has a strong impact on surface subsidence and has a controlling function for it. It was proposed that surface subsidence could be approximately predicted by calculating the UTHS subsidence.

In this work, the UTHS movement characteristics were studied using Winkler's theory of beams on an elastic foundation, the subsidence prediction equation of the main sections in the strike and dip directions was obtained under different mining dimensions, and the subsidence prediction equation of any arbitrary cross section parallel to the two main sections was established. Then, the surface subsidence prediction method for coal mining with the presence of UTHS was developed.

The Tingnan Coal Mine was taken as an example, and the subsidence curves of the strike and dip main sections were calculated using different mining dimensions. The surface reached sufficient mining when the mining region reached

1350 m in both strike and dip directions, which is much larger than the empirical range of 657–766 m (1.2–1.4 times the mining depth of the seam). Subsequently, the surface subsidence after the mining of working faces 204, 205, 206, and 207, respectively, was predicted, and the prediction method was verified by comparing the results with the measured surface subsidence results of working faces 204, 205, and 206.

The influences of UTHS thickness, strength, and layer position on the surface subsidence were discussed when main section II of the Tingnan Coal Mine reaches sufficient mining and main section I has a mining dimension of $L_1 = 660$ m. There are significant differences in the surface subsidence curves under different UTHS thicknesses, strengths, and layer positions, and variations in overburden strata compositions have a strong impact on surface subsidence. The greater the UTHS thickness or strength, the greater the range of surface subsidence and the lower the maximum surface subsidence value. When the distance between UTHS and seam increases, the maximum surface subsidence value decreases significantly and the range of surface subsidence increases slightly.

Data Availability

The data used to support the findings of this study are available from the corresponding author upon request.

Conflicts of Interest

The authors declare that there are no conflicts of interest regarding the publication of this paper.

Acknowledgments

The authors gratefully acknowledge the financial support from the Open Fund of State Key Laboratory of Groundwater Protection and Utilization in Coal Mining (grant no. SHJT-16-30.11).

References

[1] F. G. Bell, T. R. Stacey, and D. D. Genske, "Mining subsidence and its effect on the environment: some differing examples," *Environmental Geology*, vol. 40, no. 1-2, pp. 135–152, 2000.

[2] Y. H. Zhao, S. R. Wang, P. Hagan, L. W. Ren, and Z. S. Zou, "Pressure-arching characteristics in roof blocks during shallow coal mining," *Advances in Civil Engineering*, vol. 2018, Article ID 6817059, 12 pages, 2018.

[3] F. T. Wang, Q. Ma, G. Li, C. G. Wu, and G. L. Guo, "Overlying strata movement laws induced by longwall mining of deep buried coal seam with superhigh-water material backfilling technology," *Advances in Civil Engineering*, vol. 2018, Article ID 4306239, 10 pages, 2018.

[4] P. Xu, M. X. Zhang, Z. B. Lin, Z. Z. Cao, and X. Chang, "Additional stress on a buried pipeline under the influence of coal mining subsidence," *Advances in Civil Engineering*, vol. 2018, Article ID 3245624, 16 pages, 2018..

[5] A. O. Altun, I. Yilmaz, and M. Yildirim, "A short review on the surficial impacts of underground mining," *Scientific Research and Essays*, vol. 5, no. 21, pp. 3206–3212, 2010.

[6] L. Nie, H. Wang, and Y. Xu, "Application of the arctangent function model in the prediction of ground mining subsidence deformation: a case study from Fushun City, Liaoning Province, China," *Bulletin of Engineering Geology and the Environment*, vol. 76, no. 4, pp. 1383–1398, 2017.

[7] S. Knothe, "Observations of surface movements and their theoretical interpretation," in *Proceedings of the European Congress on Ground Movement*, pp. 210–215, Leeds, UK, April 1953.

[8] J. Litwiniszyn, "The theories and model research of movements of ground masses," in *Proceedings of the European Congress on Ground Movement*, pp. 206–209, Leeds, UK, April 1957.

[9] B. S. Liu and G. H. Liao, *Basic Law Governing Ground Movement in Coal Mines*, Coal Industry Press, Beijing, China, 1965.

[10] National Coal Board (NCB), *Subsidence Engineer's Handbook*, NCB Mining Department, London, UK, 1975.

[11] H. Kratzsch, *Mining Subsidence Engineering*, Springer-Verlag, Berlin, Germany, 1983.

[12] S. S. Peng and H. S. Chiang, *Longwall Mining*, Wiley, New York, NY, USA, 1984.

[13] G. Ren, D. J. Reddish, and B. N. Whittaker, "Mining subsidence and displacement prediction using influence function methods," *Mining Science and Technology*, vol. 5, no. 3, pp. 89–104, 1987.

[14] G. Q. He, L. Yang, G. D. Ling, F. C. Jia, and D. Hong, *Mining Subsidence Science*, China University of Mining & Technology Press, Xuzhou, China, 1991.

[15] P. R. Sheorey, J. P. Loui, K. B. Singh, and S. K. Singh, "Ground subsidence observations and a modified influence function method for complete subsidence prediction," *International Journal of Rock Mechanics and Mining Sciences*, vol. 37, no. 5, pp. 801–818, 2000.

[16] X. Cui, J. Wang, and Y. Liu, "Prediction of progressive surface subsidence above longwall coal mining using a time function," *International Journal of Rock Mechanics and Mining Sciences*, vol. 38, no. 7, pp. 1057–1063, 2001.

[17] M. I. Álvarez-Fernández, C. González-Nicieza, A. Menéndez-Díaz, and A. E. Álvarez-Vigil, "Generalization of the n-k influence function to predict mining subsidence," *Engineering Geology*, vol. 80, no. 1-2, pp. 1–36, 2005.

[18] C. Gonzalez-Nicieza, M. I. Alvarez-Fernandez, A. Menendez-Diaz, and A. E. Alvarez-Vigil, "The influence of time on subsidence in the Central Asturian Coalfield," *Bulletin of Engineering Geology and the Environment*, vol. 66, no. 3, pp. 319–329, 2007.

[19] H. Xu, B. Liu, and Z. Fang, "New grey prediction model and its application in forecasting land subsidence in coal mine," *Natural Hazards*, vol. 71, no. 2, pp. 1181–1194, 2014.

[20] L. Nie, H. Wang, Y. Xu, and Z. Li, "A new prediction model for mining subsidence deformation: the arc tangent function model," *Natural Hazards*, vol. 75, no. 3, pp. 2185–2198, 2015.

[21] C. C. He and J. L. Xu, "Subsidence prediction of overburden strata and surface based on the voussoir beam structure theory," *Advances in Civil Engineering*, vol. 2018, Article ID 2606108, 13 pages, 2018.

[22] F. Wang, S. J. Chen, J. L. Xu, and M. Z. Ren, "New method to design coal pillar for lateral roof roadway based on mining-induced stress: a case study," *Advances in Civil Engineering*, vol. 2018, Article ID 4545891, 13 pages, 2018.

[23] A. Asadi, K. Shakhriar, and K. Goshtasbi, "Profiling Function for Surface Subsidence Prediction in Mining Inclined Coal Seamsfiling function for surface subsidence prediction in

mining inclined coal seams," *Journal of Mining Science*, vol. 40, no. 2, pp. 142–146, 2004.

[24] D. Xuan, J. Xu, and W. Zhu, "Dynamic disaster control under a massive igneous sill by grouting from surface boreholes," *International Journal of Rock Mechanics and Mining Sciences*, vol. 71, pp. 176–187, 2014.

[25] Z. Chang, J. Wang, M. Chen, Z. Ao, and Q. Yao, "A novel ground surface subsidence prediction model for sub-critical mining in the geological condition of a thick alluvium layer," *Frontiers of Earth Science*, vol. 9, no. 2, pp. 330–341, 2015.

[26] M. G. Qian, X. X. Miao, J. L. Xu, and X. B. Mao, *Study of Key Strata Theory in Ground Control*, China University of Mining & Technology Press, Xuzhou, China, 2003.

[27] State Bureau of Coal Industry, *Regulations of Coal Pillar Design and Extraction for Buildings, Water Bodies, Railways, Main Shafts and Roadways*, Coal Industry Press, Beijing, China, 2000.

[28] G. R. Feng, P. F. Wang, Y. P. Chugh et al., "A coal burst mitigation strategy for tailgate during deep mining of inclined longwall top coal caving panels at Huafeng coal mine," *Shock and Vibration*, vol. 2018, Article ID 5929785, 18 pages, 2018.

[29] R. N. Gupta and A. K. Ghose, "Strata support interaction on a powered support longwall face under a massive dolerite sill-a study," in *Proceedings of the 11th International Conference on Ground Control in Mining*, pp. 140–149, Wollongong, Australia, July 1992.

[30] W. Yang and X. Xia, "Prediction of mining subsidence under thin bedrocks and thick unconsolidated layers based on field measurement and artificial neural networks," *Computers & Geosciences*, vol. 52, pp. 199–203, 2013.

[31] Y. W. Shi, "Analytical calculations of abutment pressure," *Journal of China Coal Society*, vol. 18, no. 6, pp. 1–10, 1993.

[32] C. He, J. Xu, F. Wang, and F. Wang, "Movement boundary shape of overburden strata and its influencing factors," *Energies*, vol. 11, no. 4, p. 742, 2018.

[33] J. Q. Jiang, *Stress and Movement of Surrounding Rock*, Coal Industry Press, Beijing, China, 1993.

[34] J. X. Zhang, J. Li, T. L. An, and Y. L. Huang, "Deformation characteristic of key stratum overburden by raw waste backfilling with fully-mechanized coal mining technology," *Journal of China Coal Society*, vol. 35, no. 3, pp. 357–362, 2010.

[35] J. X. Zhang, M. Li, Y. L. Huang, and L. Y. Li, "Interaction between backfilling body and overburden strata in fully mechanized backfilling mining face," *Disaster Advances*, vol. 6, pp. 1–7, 2013.

[36] Y. Q. Long, *Computation of Elastically Supported Beams*, People's Education Press, Beijing, China, 1981.